IEEE Access
Multidisciplinary | Rapid Review | Open Access Journal

Received January 5, 2021, accepted January 13, 2021, date of publication January 19, 2021, date of current version January 27, 2021.

Digital Object Identifier 10.1109/ACCESS.2021.3052964

Method for the Optimal Positioning of the Cutter at the Honeycomb Block Cutting Applying Computer Vision

MAKSIM V. KUBRIKOV[1], MIKHAIL V. SARAMUD[1,2], AND MARGARITA V. KARASEVA[3,4]

[1]Research Laboratory of Robotic Systems, Reshetnev Siberian State University of Science and Technology, 660037 Krasnoyarsk, Russia
[2]Department of Informatics, Institute of Space and Information Technologies, Siberian Federal University, 660041 Krasnoyarsk, Russia
[3]Department of Systems Analysis and Operations Research, Reshetnev Siberian State University of Science and Technology, 660037 Krasnoyarsk, Russia
[4]Department of Digital Technologies of Management, School of Business Management and Economics, Siberian Federal University, 660041 Krasnoyarsk, Russia

Corresponding author: Mikhail V. Saramud (msaramud@gmail.com)

This work was supported by the Ministry of Science and Higher Education of the Russian Federation under Contract FEFE-2020-0017.

ABSTRACT The problem of optimal cutting of honeycomb blocks is considered in the article. The urgency of using irregular shapes application cutting from honeycomb blocks made of modern composite materials is substantiated. The problem is to obtain a cut of a given shape from honeycomb blocks. The optimal cutting plane of the single cell face of a honeycomb block is found on the basis of calculations for the stability and stretching force in adjacent faces applying a finite element method. The problem of obtaining faces and nodal points of a honeycomb block when calculating the coordinates of the optimal cut points of a real honeycomb block using machine vision methods. The most suitable algorithms, a part of the OpenCV library, are considered. The authors decided to develop their own algorithm for recognizing an irregular cellular structure since the existed algorithms did not solve the stated problem. As opposed to existing algorithms, the proposed one finds all the nodal points and faces even on the deformed sections of the honeycomb block avoiding false faces. The method helps to find coordinates of all nodal points and determine the connection of adjacent points with a face. As a result, real faces, not perfect geometrically, are replaced by line segments. The test result proves its correctness and practical applicability. The proposed method solves an optimal cutting problem of aluminum honeycomb block. It should be noted that the proposed method is customizable and can be applied to any honeycomb or cellular panels.

INDEX TERMS Image recognition, composite materials, cutting tools, machine vision.

I. INTRODUCTION

In the modern aerospace industry, sealed structures of titanium and aluminum satellites are being replaced by lighter ones based on non-hermetic constructions made of composite materials [1]–[4]. The satellite platform consists of flat sandwich panels. Each panel contains two outer layers of carbon fiber sheets (a few millimeters thick) and the honeycomb between them [5], [6]. Such honeycomb panels have high strength, rigidity and low weight [7]. Inserts are provided in the internal structure of honeycomb panels for fixing satellite elements. A portion of the honeycomb is removed for the placement of the inserts with end milling or side milling cutters. However, this material has poor processing ability [8]–[10], and resulting defects significantly limit its application. This problem arises because of the cellular and thin-walled structure and, as a consequence of weak rigidity in the plane direction of cellular materials [11], [12]. Provision of a geometrically complex shape and size of a honeycomb panel can be achieved through the efficient processing. Therefore, characteristics of the cutting process and the influence of processing parameters are important [13].

In the course of the investigation, the insufficient problem development concerning the buckling-free vertical cutting of honeycomb blocks was revealed. Although, the wedge cutting and bursting action at indenting honeycomb blocks has been extensively studied, some problems persist. The main problem of obtaining a high-quality cut, without slivers and deformations of a thin-walled cellular structure, is a correct selection of the cutting site. The optimal point and angle of cut determination on a real object is a complex problem, because of the irregular honeycomb structure. Currently, it has not been sufficiently considered and solved by researchers.

The article considers a finite element model of various cutting points. The most optimal position of the cutter is determined on the basis of the obtained model. The method

The associate editor coordinating the review of this manuscript and approving it for publication was Shuihua Wang.

has been developed to determine an irregular cellular structure of a real object and develop its digital twin. On the basis of machine vision, the vertices and faces of the honeycomb block were found; it allows to determine machine coordinates for positioning a cutter relatively to the optimal cutting points.

II. RELATED WORKS

Some investigations have been carried out to study the honeycomb panels processing. In [14] typical defects of machining are presented and the processing characteristics of honeycomb block are studied. Cutting defects and slivers on the panels are considered; their locations are determined. A cutting force model for predicting the milling force at different spindle speeds, feed and cutting angle is considered.

The effect of the cutting force at ultrasonic cutting as the most important physical quantity is considered in the article [15]; the processing state of a honeycomb block is presented. The influence on the cutting force at fixing honeycomb composites on the working place, the quality of the processed surface and the service life of the cutter are shown. A theoretical model of ultrasonic processing of honeycomb blocks was developed. Some experiments are presented and the effect of cutting depth, deflection angle and inclination angle on the cutting force is analyzed. The material shows a detailed investigation of the mechanism and parameters of ultrasonic cutting of honeycomb cores.

The results of the experiments are presented in the article [16]. The analysis of a 3D-FE model of the aluminum honeycomb ultrasonic cutting with a disc blade applying commercial software ABAQUS are provided. The detailed conditions of contact between the cutting blade and the honeycomb block, the distribution of stresses in the cutting zones and the morphology of the honeycomb structure after cutting were analyzed and simulated on the basis of the developed model.

The researchers in the article [17] investigate the effect of a cell size on the cutting ability of hexagonal thin-walled aluminum honeycombs cut with a wide blade under quasi-static compression.

The problem of faces detection in a color image is considered in the article [18]. The morphological multilevel fuzzy face detection scheme (MMFED) is proposed. It was compared with the operator Sobel, FMFED, proposed by J. Wu, Z. Yin and Y. Xiong in the article [19]. The experimental results show that the application of morphological transformations helps to find more accurate and clear faces of color images.

The method for detecting and identifying cutting lines, based on the allocation of two faces applying the Hough transform is proposed in the article [20]. In this article, the algorithm copes well with determining both straight segments and bends by determining the direction of the bend of the curve, highlighting the characteristic points of the curve and approximating the least squares method.

The article [21] is also devoted to finding a face weld and it notes the efficiency of the morphology application.

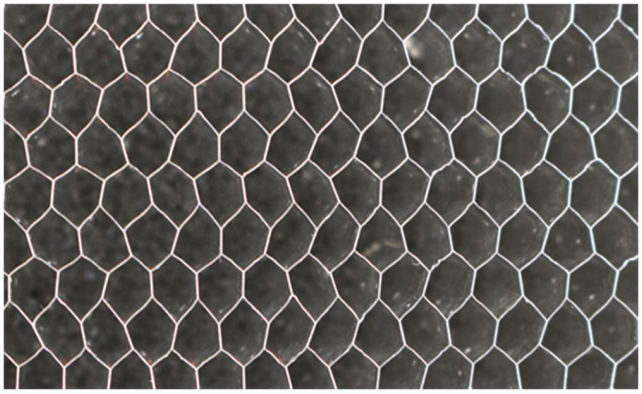

FIGURE 1. Original image of the block.

A. INVESTIGATION OF THE EXISTED ALGORITHMS

The honeycomb block is fixed on the working surface for the cutting process mechanism. The video equipment is applied for obtaining an image of the cellular structure of a honeycomb block. Also, machine coordinates are transported in the process of image transmission. It makes possibility to bind a digital model of the honeycomb block to a real object.

When the image of the honeycomb block is received and processed, binarization of the image is carried out. As a result, the faces are marked in white, and the internal volume of the cells is presented in black.

Additional transformations (morphology) are performed on the image to improve the quality of algorithms.

B. HOUGH TRANSFORMATION METHOD

In our previous article [22] we studied the possibility of edge detection with the help of the Hough transform method [23]; however, it did not give positive results.

The recognition methods did not show any satisfactory result because of the presence of a large number of faces with defects both in a real object and when additional transformations of the original image were obtained. So, it was decided to recognize nodal points of the cells and build faces on their own. The result of the method is an array of nodal points and a set of faces between them. With the help of this approach, an approximate digital model of the honeycomb block was obtained. This method allows to obtain high accuracy of positioning of the cutter with a high resolution of the image.

The methods implemented in the openCV library were studied to determine vertices. This library implements three methods for angles determination, the Harris [24], [25], Shi-Tomasi [26], FAST (Features from Accelerated Segment Test) [27] methods. The original image of a honeycomb block is shown in Figure 1. According to the figure, a real honeycomb structure is irregular; some faces are not straight or have physical defects. Also, additional defects are results of optical distortions arising while making images.

C. HARRIS METHOD

The Harris detector is a modification of the Moravec detector, since it is characterized by anisotropy.

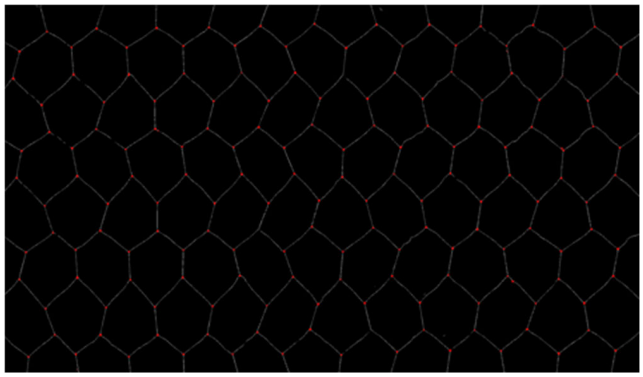

FIGURE 2. Harris method.

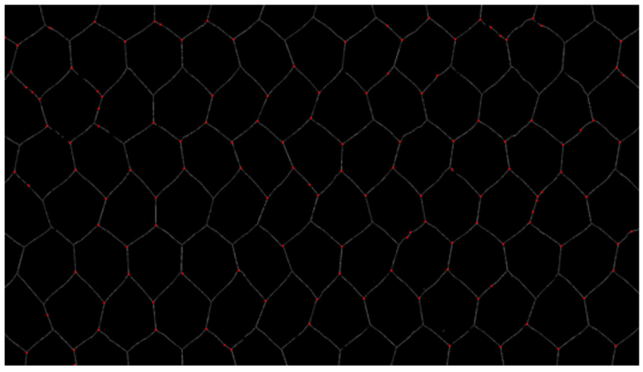

FIGURE 3. Shi-Tomasi method.

The original image to binarization and morphological operations (two cycles of erosion and topological skeleton) is exposed to improve the result. We apply the Harris method to the resulting image presented in Figure 2.

D. SHI-TOMASI METHOD

The Shi-Tomasi algorithm is a modification of the Harris algorithm. We apply the same processing to the original image as in the Harris method for better detection. The result of the Shi - Tomasi method is given in Figure 3.

E. FAST METHOD

Rosten and Tom Drummond (2005) introduced a rather successful FAST (Features from Accelerated Segment Test) algorithm.

Initially, the original image must be binarized, the morphology is not applied. This leads to a large number of false positives. The result of the FAST algorithm running is shown in Figure 4.

III. FINDING AN OPTIMAL CUTTING PLANE OF HONEYCOMB BLOCKS EXAMINED FOR STABILITY AND STRETCHING FORCE IN ADJACENT FACES

The problem of finding the optimal cutting plane of the cellular structure of a honeycomb block is considered. The Femap with Nastran software [28], [29] was applied to solve the problem by a numerical method. Elements of the plate type were selected for the model of a honeycomb cell. The wall thickness was set equal to 0.05 mm, the side length of the honeycomb cell was 5 mm, and the height was 50 mm.

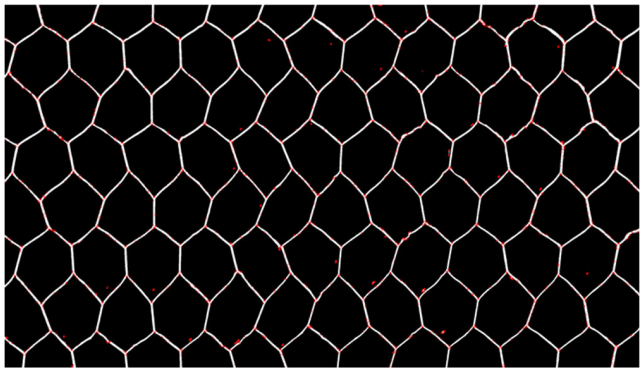

FIGURE 4. FAST method.

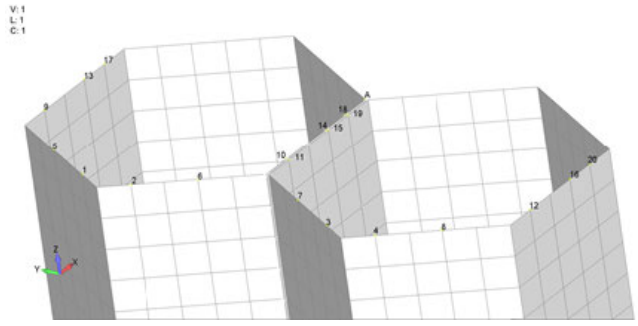

FIGURE 5. Points of loads application at five stages of analysis.

The material of the honeycomb model was an aluminum alloy 3003. Mechanical properties of the honeycomb material are as follows: Elastic modulus, E = 69 GPa, density ρ = 2730 kg/m^3, Poisson ratio $\mu = 0.33$, conditional flow stress $\sigma_{0.2} = 85$ MPa.

The stability analysis was performed for five sets of loads. Each set included four points that corresponded to five YZ cut planes (Figure 5). At each step a concentrated load was applied at each of the four points. Fixations were made: rigid fixation along the bottom faces of the cells and fixation along displacements lengthwise the transverse faces of the model.

A distribution picture of the stress intensity and displacement was obtained for each study of the points array. A cut of nodal points 13-16 is the most promising one (Figure 6).

The values of the buckling load Fbuck were obtained. The loss of stability occurs and the block acquires a new curvilinear shape relative to the cutting points with distance from the nodal point A (Figure 5).

On the basis of the given calculations it is possible to summarize, that if we take into account the loss of stability, the cutting points along the faces parallel to the X axis will be optimal. Meanwhile, the minimum value of F_{buck} for these cases is observed along the array of 13-16 points. The investigation concerning the stretching force arising at the adjacent faces of the honeycomb block cells showed that the smallest stretching force also occurs along the array of 13-16 points. So, we can conclude that the optimal points for cutting are points for cutting along an array of 13-16 points. In our particular case it corresponds to the shift of 2 mm from the cell nodal point or about 0.4 of the face length in a general case.

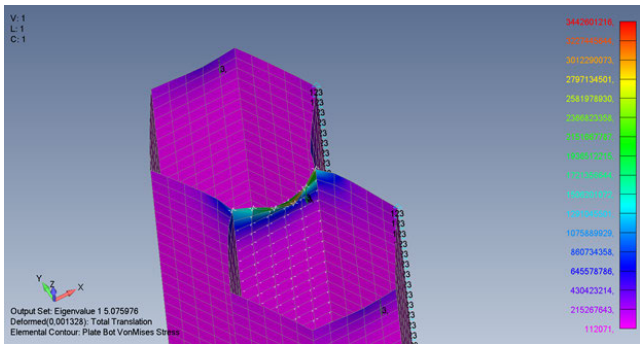

FIGURE 6. Loss of stability under loading at different points.

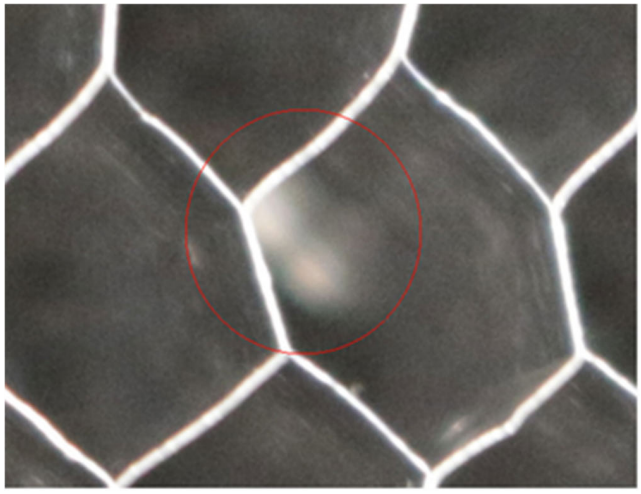

FIGURE 7. Image defect.

IV. ANALYSIS OF THE ALGORITHMS RUNNING FOR IMAGES WITH A DEFECT

A defect in the original image is shown in Figure 7. There is a defect in the cell structure that reflects light. As a result, the brightness of this segment is comparable to the brightness of the face, and after the image binarization; this site is white.

None of the methods described above finds this vertex because of this defect. The operation of three methods on this fragment of the image is shown in Figure 8.

These three methods have been examined by us. The Harris method gives the highest percentage of detected vertexes and a very low percentage of detecting false vertexes, the Shi-Tomasi method does not find all true vertexes; it gives some false positives. The FAST method also finds a high percentage of true vertices, but it also gives a very large number of false positives. According to the comparative analysis one can conclude that the Harris method is the most applicable method for our problem solving. The results are given in Table 1. However, all the presented algorithms do not give an ideal result on the studied images.

According to the result of the experiment, none of the algorithms showed a satisfactory result on the test image. In the segment shown in Figure 8; none of the algorithms recognized a vertex correctly. For this reason, we have developed a new method developed to determine the nodal

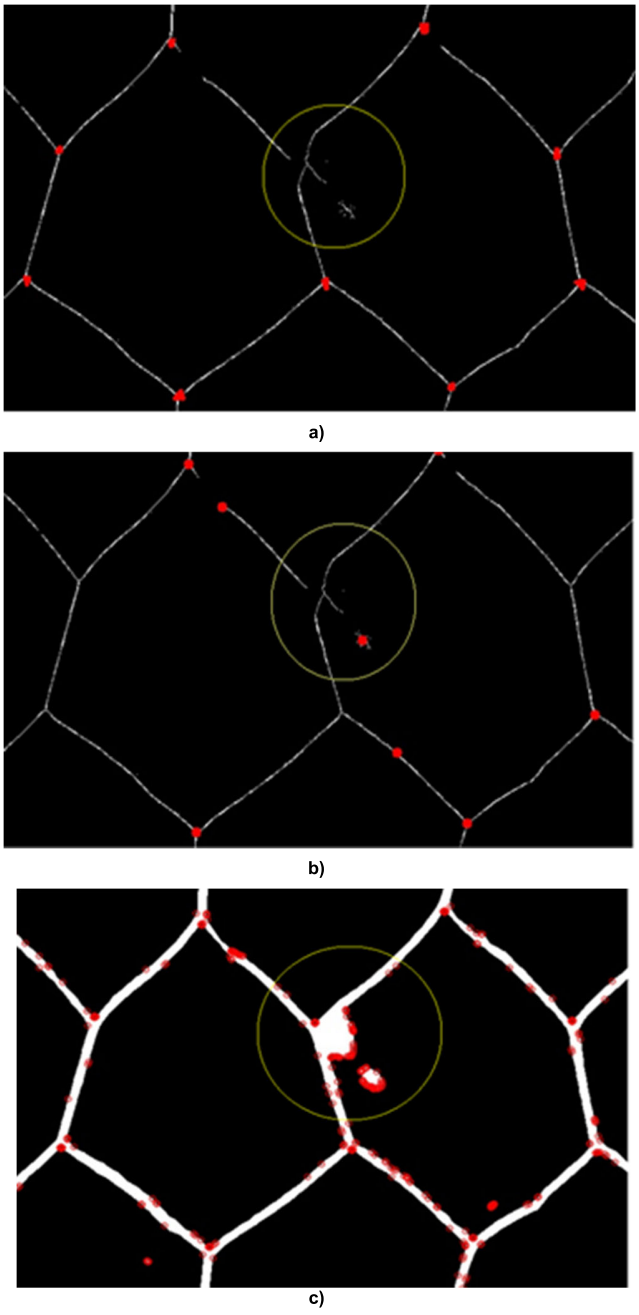

FIGURE 8. a) Harris Method b) Shi - Tomasi Method c) FAST Method.

points of irregular integral structures, including honeycomb structures.

V. METHOD FOR DETERMINING NODAL POINTS, FACES AND CUTTING POSITIONING

The proposed method is a set of steps with intermediate results presented in the form of images and data sets. These steps are described further.

A. STEP 1

The first step is to pass through all processed images a pixel by pixel. We check if the given pixel is not black (*all(img[x,y] >= [180,180,180])*) at each pixel. If a pixel is black, then we move on to the next one. If a pixel is not black, then we call the

TABLE 1. Research results.

Features	Harris Method	Shi-Tomasi Method	FAST Method
Vertex detection	> 90 %	< 70 %	> 90 %
False detection	low (detected false vertices <3 for 5 cells)	high (detected false vertices >3 but <6 for 5 cells)	very high (detected false vertices > 6 for 5 cells)
Effect of binarization	helps in detecting not significantly	helps in detecting significantly	helps in detecting significantly
Binarization + morphology	helps in detecting significantly	helps in detecting significantly	degrades detection, adds false positives
Image quality	helps in detecting significantly	helps in detecting significantly	helps in detecting significantly

developed function *node_multiaxial()*. This function builds a set of points around the selected pixel located on a circle around the studied pixel. Imagine a clock with an arrow as an example. The first pixel of the circle will be at three o'clock, the next pixel of the circle will be shifted clockwise by an angular step, depended on the wall thickness of the block (in pixels) and set by a step along the circle L. It is recommended to select a step value no more than 0.8 of the line width. A step is set so that it is guaranteed not to miss the line, but at the same time, not to increase the intensity too much. A circle radius R is selected in the range from 0.1 to 0.3 of the average length of the face to ensure that any two nodal points are not captured. In our case the radius is equal to 30 pixels. With an average line width of 11 pixels, we chose a step of 7 pixels. It gives the circular a shift of 14°. We pass the required shift in pixels to the function; and it is recalculated to the angular step dlt_a = (L*360) / (2*math.pi*R). It is checked again whether a pixel is not black at each step, at a pixel on the studied circle. If it is not black, then go to the next point with a standard step L. If a white pixel is detected, then a face is found. We increase an indicator of the detected faces number by a value of the face counter K of the detected faces in 1 and go to the next point on the circular with an increased step L * jump, where jump is a variable that sets how many times a "jump" from the found face will be greater than a standard step on the circular.

A "jump" is introduced to optimize the algorithm, since there is no next face at the jump distance. For example, in the image under consideration, the average thickness of faces is 11 pixels, and the standard step is 7 pixels. This value guarantees us that a face will not be missed; however, there is a probability to find the same face on the circular after 7 pixels without a "jump" mechanism. We find a face with the help of a "jump" and after that we "jump" not in 7, but in 28 pixels from the found point (a "jump" is equal to 4). So, it will help us to get out of the site of the found face and exclude false double positives. However, we do not select too large value not to miss the next face located close to the studied one due to a violation of the block geometry.

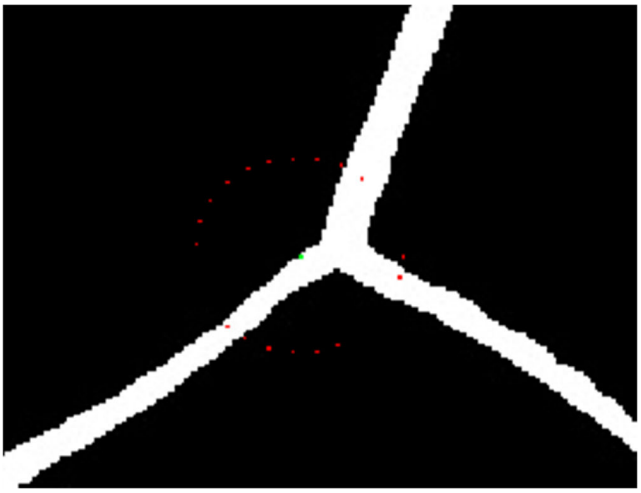

FIGURE 9. Visualization of the investigation at points of a circle.

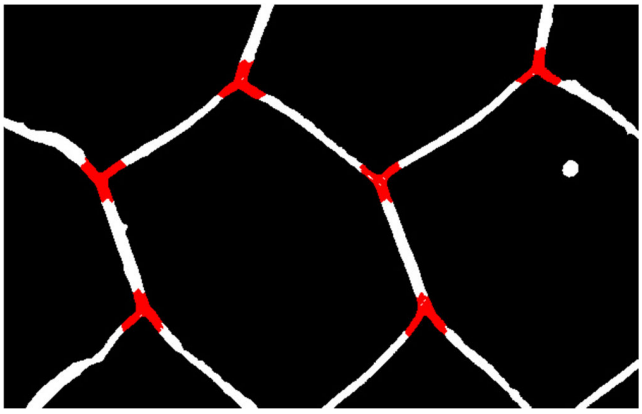

FIGURE 10. Visualization of the first step.

The check visualization along a circle is given in Figure 9. The faces of the honeycomb blocks after binarization of the image are white, a center pixel is green (not a black pixel of the image found during investigation), red pixels are the ones on the circle that we are investigating.

A starting point is located at 3 o'clock. We find a face by the second point, remember it and make a jump. Then, we investigate the next points, and we find a face at point 6 again, remember it and make a jump. A cell node has 3 faces. As a result, at 10 points we find the third face, whereas, a face counter K becomes equal to 3. In our case it is a condition for leaving a cycle.

After we have found three faces, a cycle stops and a function returns TRUE, indicating that a selected point is included in the nodal zone, since three faces intersect a circle around it. If we have passed all the points of the circle, and met less than three faces, a function returns FALSE; it means that this area is not a node, but it is located on the face.

For illustrative purposes, an additional visualization was made in Figure 10, i.e., the found pixels in the original image were painted in red.

We create two additional images filled with black pixels completely. They match the original size (let's call them img 1 and img 2).

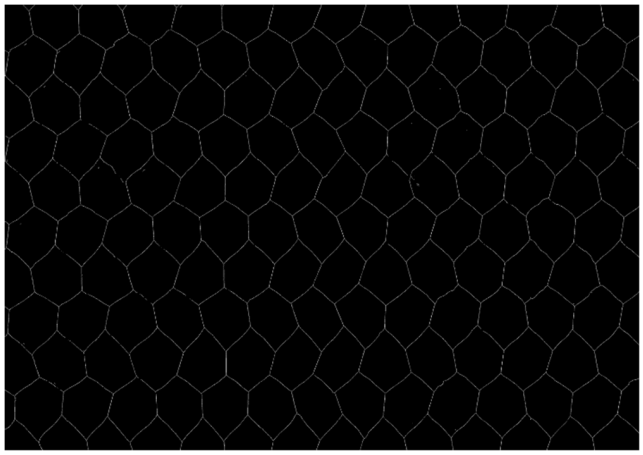

FIGURE 11. Original image after processing.

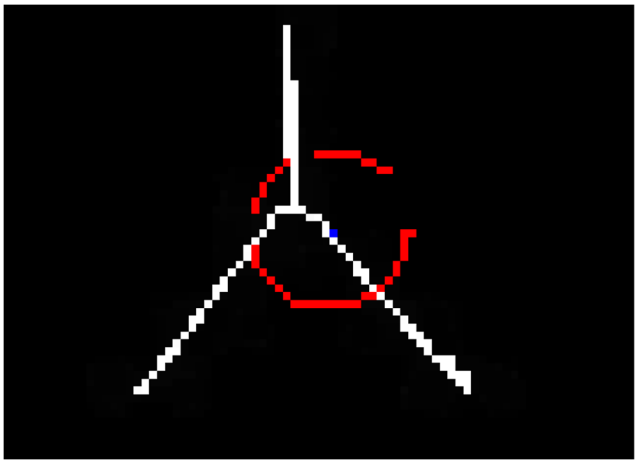

FIGURE 12. Pixels pass a thin face.

If the function returns TRUE, then we change the color of the pixel with the given coordinates in img1 to white. As a result, we get tan image img1, which contains all the nodal points and face segments of the length no more than R (corresponds to the red areas in Figure 12).

B. INVESTIGATION OF MORPHOLOGY INFLUENCE ON RUNNING

We worked with the original image after binarization. However, it is possible to perform additional transformations on the binarized image, such as erosion and stretching.

The transformations made it possible to obtain an image with a face thickness of 1-2 pixels. The resulting image is shown in Figure 11.

Repeat all the operations for the given image and compare the results and the runtime. The node_multiaxial() function will be fulfilled 10 times less since there are almost 10 times fewer pixels on the faces. However, now we need to validate points on a circle and a step of 1 pixel, or, in our case, 2°. It will increase the operation time of the function 7 times.

It was understood after the test validation that the function of finding pixels on a circle does not work correctly with such thin lines, since even with a step of 1 pixel, a line perpendicular to a segment of a circle may not be detected (Figure 12).

C. RUNTIME OPTIMIZATION

The experiments had been conducted and it became clear that thin lines can significantly reduce calls of the *node_multiaxial()* function. However, the function itself works correctly only with thicker faces. The following algorithm of image processing was proposed to accelerate its runtime. The image with thin faces is used to determine what pixel is applied to call the test validation function; the test validation runs from this pixel of the image with thick faces. Thus, we get the correct areas of nodal points of small thickness (Figure 13), optimizing the runtime of the algorithm.

Let's return to the problematic area of the image shown in Figure 10. Our algorithm recognizes the area of the nodal point, even if one of the faces does not connect to it (Figure 14), in contrast to the existed algorithms.

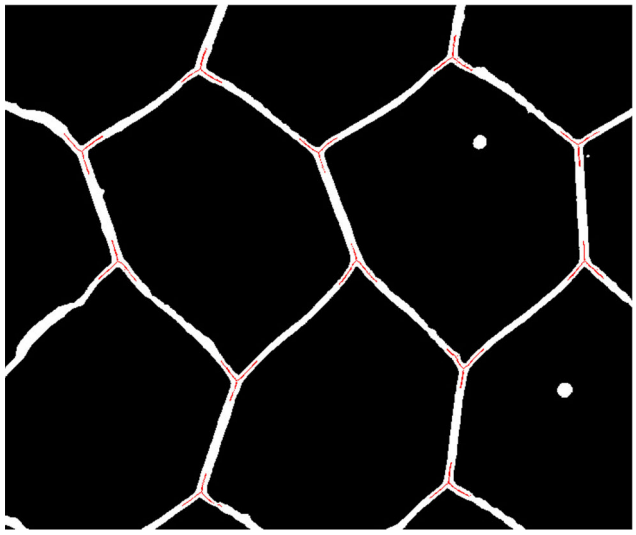

FIGURE 13. Result of the first step of the combined algorithm.

Compare the runtime of each alternative on thick or thin lines with this hybrid alternative on the same site of the image. As a result of the test validation, we got the following runtime on our image: a combined algorithm is 197 seconds, passage on thick lines is 1314 seconds, passage on thin lines is 188 seconds. All results in the article were obtained on a CPU Intel Core i3-4170 @ 3.70GHz.The results show that the application of the image with thin faces to determine the points to call the test validation function, and its runtime on thick faces determines the sites at the nodal points correctly. It improves the runtime significantly.

D. STEP 2

After that, we carry out the same operations for img1 as at step 1, and put down the found points for img2. So, we work with the accelerated algorithm; we look for white pixels in the picture with thin faces. The intersections with thick faces are investigated in the picture. Thus, the algorithm processes the

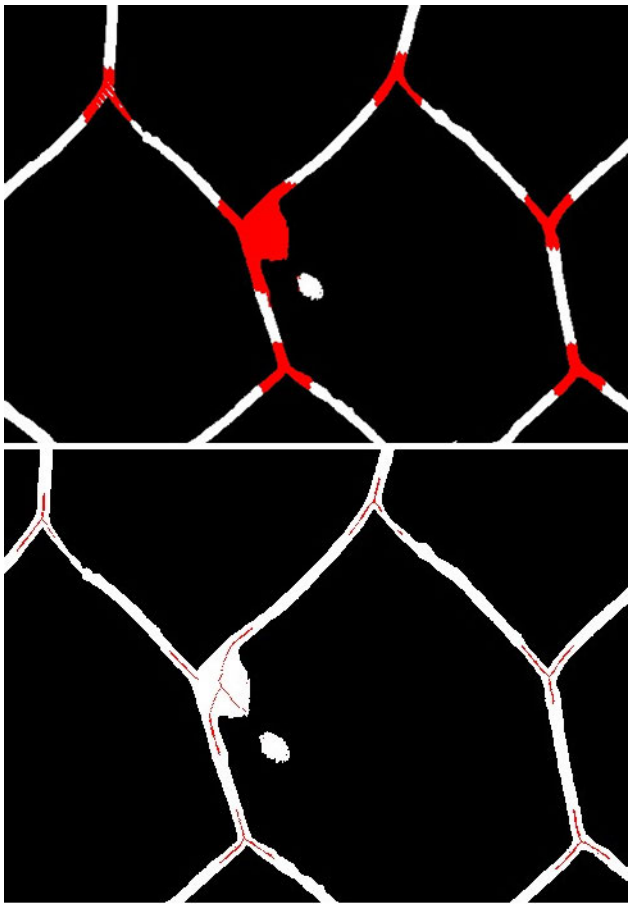

FIGURE 14. Buckling site processed by the first step of the algorithm.

entire image rather quickly. But the found node areas have a thickness of 1 pixel and the problem described earlier arises with their processing. We increase the thickness of faces to solve this problem. For this purpose we expand the matrix of 5×5 pixels over the image for one iteration. As a result, a search function runs correctly with thicker lines.

Some parts of the faces that are more than R from the nodes are absent in img1. Only points belonging directly to the nodes, not face segments, capturing the extreme points of the remaining 3 faces by a circle, pass the test validation. The points on the faces will not pass the test validation, since a circle will not capture pixel 3 of this face itself, since this face is cut in R from the node. According to the result of experiments, the optimal solution reduces the radius 3 times.

In our experiment we reduced the radius from 30 to 10 pixels; so, a step was 3 pixels, a jump was 4. The result of the work is shown in Figure 15. Faces remaining after the first step are shown in white; faces found at the second step are presented in red.

As a result, we got only pixels in the area of nodal points, but we are to get specific coordinates. So, we will process the image further.

We select the contours of the red sites by the function *contours0, hierarchy = cv.findContours(thresh. copy(), cv.RETR_TREE, cv.CHAIN_APPROX_SIMPLE)* in

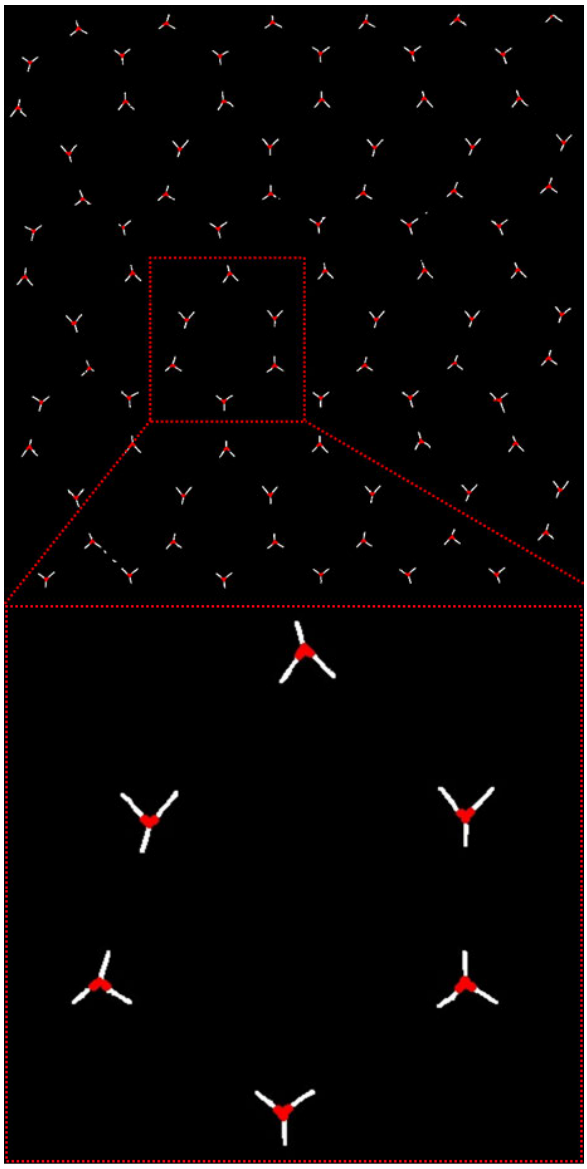

FIGURE 15. Fragment of img2 after the second step.

img2 (Figure 17). Then, we find the ellipses for the resulting contours.

As a consequence, we get coordinates of the ellipses centers; they are our nodal points.

Now we build the visualization in Figure 16 for better understanding. The ellipses with the found points are shown in green, and their centers are in blue. As a result, we got an array of all nodal points with their coordinates.

E. STEP 3

We got a list of all the vertices. Therefore, a task of faces determination arises. Since real faces do not have an ideal shape, we replace them with line segments that have start and end coordinates at the real nodal points.

First, we test the found points at a certain distance from each other for problem solving. If we have a rather regular-shaped block without buckling, a distance test finds

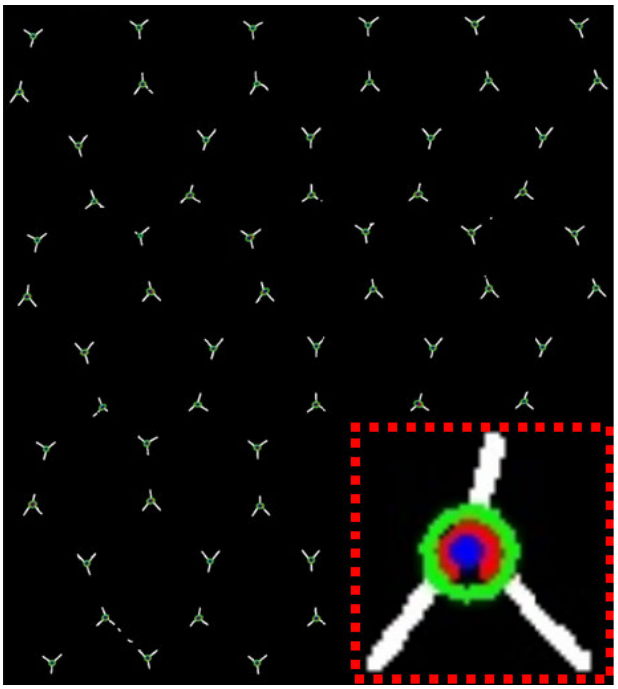

FIGURE 16. Visualization of the search for vertices of faces as an ellipses center.

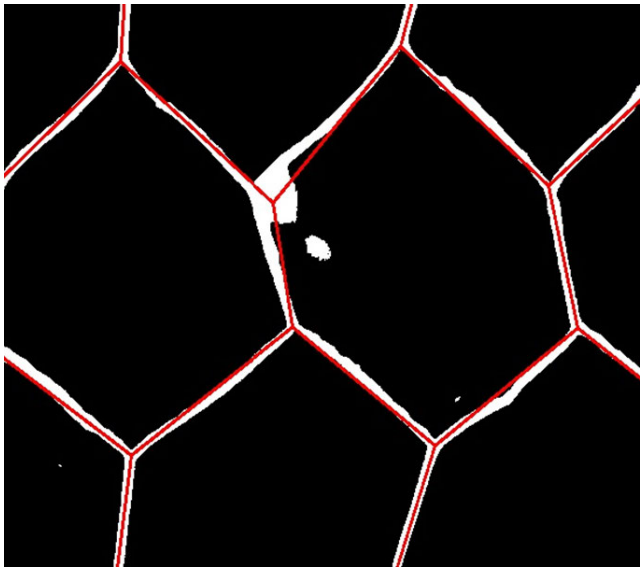

FIGURE 17. Instance of replacing real faces with segments on a buckling site.

all the faces correctly. However, such a test validation is not reliable enough and does not work correctly on segments with buckling. Therefore, we take a larger range of acceptable distances between nodes and test several segments between the selected nodes once more. If a distance between nodes satisfies the condition, then we test 3 matrixes on the segment between the nodes. They are: a midpoint of the segment, a 1/5 length of the segment, and a 4/5 length of the segment. We test an 8×8 pixel area around each of these three points for non-black pixels. If such pixels are found in at least 2 of 3 sites, then the specified points are connected by a face.

TABLE 2. Algorithm results.

Image №	Method	True points	False points	Missing points
1	Our method	85	0	0
	Harris	85	0	0
	Shi-Tomasi	42	44	43
2	Our method	99	0	0
	Harris	98	5	1
	Shi-Tomasi	50	35	49
3	Our method	125	0	1
	Harris	124	4	2
	Shi-Tomasi	50	12	61
4	Our method	123	0	0
	Harris	122	10	1
	Shi-Tomasi	59	25	64
5	Our method	220	0	0
	Harris	217	13	3
	Shi-Tomasi	137	54	83

So, we add it to a face array. If there are only black pixels in the specified sites, then the points are not connected by a face. If non-black pixels are found in only one site out of three, we assume that an image buckling or exposure is detected inside a cell. In this case face is not taken into account. Therefore, we find all the faces of the honeycomb structure. The result is shown in Figure 17.

The result of the developed method is an array of all faces of all connected vertices. Coordinates of the resulting array are tied to the machine coordinates of the real honeycomb block.

Also we test the operation of the algorithm on the defective site.

It is important to note that the resulting algorithm is customizable and it is applicable not only for the structures considered. It can be applied to some cellular cores by changing the corresponding variables influenced by the number of faces converging at nodal points, an average length of a face, and deviations of geometric parameters.

F. COMPARISON OF ALGORITHMS

We examined the quality of our algorithm in comparison with the existing ones. So, we took 5 test images of a honeycomb block and searched for nodal points both with our algorithm and with existing ones. Image 1 is a 6×5 cells segment with many highlights, off-face areas that remained white after binarization.

Image 2 is a 7×4 cells segment with few highlights but including a defect depicted in Figures 9–10.

Image 3 is a segment of 9×4 cells with minor highlights and a few deformed edges. Image 4 is a segment of 6×6 cells with uneven edge thickness. Image 5 is a segment of 8×9 cells without significant defects. The FAST method is not included in the comparison since it has shown unsatisfactory performance. The results are given in Table 2.

According to the comparison of the results, our algorithm turns out to be much more efficient than the existing ones.

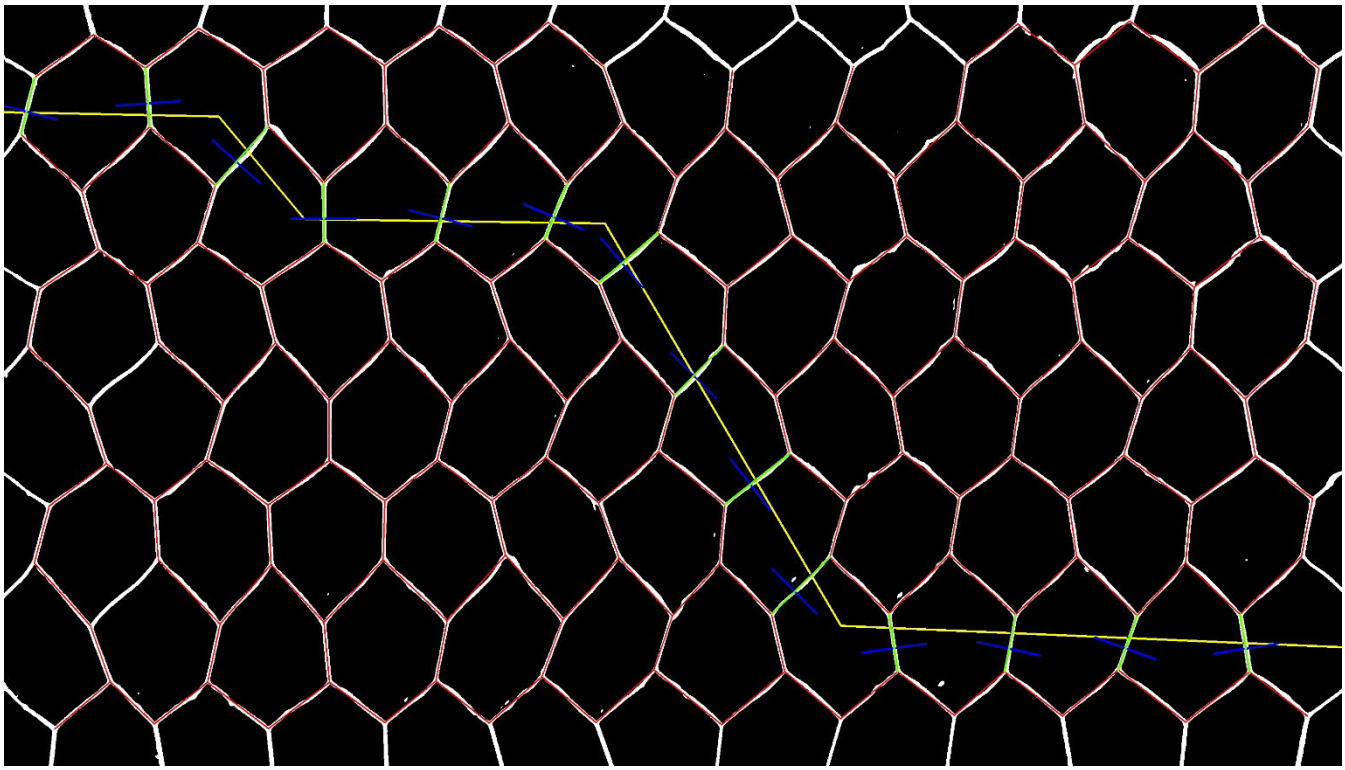

FIGURE 18. Selected points and cut angles.

In only one image, our method missed one nodal point, which was too close to the edge of the image. The line segment outgoing from it was shorter than the specified radius of the circle, so our algorithm did not find this point. It is important to note that our method does not find false nodal points by checking for the intersection of the circle with three faces.

G. CALCULATION OF CUTTING POINTS

The next step is to get a list of all the faces that our cutting line intersects. For this purpose, a profile of the cut figure is placed on the obtained digital model of the honeycomb structure, in the form of a set of rectilinear segments. Then we test the intersection of the cut line segments and our faces. Thus, we get a list of all intersecting faces and the coordinates of the intersection points. The next step is to get a list of all the faces that our cutting line intersects.

Then, we determine an optimal cutting point on the intersecting faces. The optimal point is 40% of the face length from the node of the cutting shape. In other words, no matter where a cutting line intersects a face; we make a cut only at the optimal point, leaving 2 mm near the face on the side of the cutting shape. A cutting angle is chosen perpendicular to the cutting face. A blade is located in the middle area of the cutting point. The cutting point of the face moves 2 mm from the midpoint of the blade for more regular wear on the cutting edge. The width of the blade is 5 mm, the thickness is 0.5 mm. It has a double-sided sharpening at an angle of 30°.

An additional test validation is made. The blade at this point mustn't intersect other faces, except for the cutting one. Due to the irregular geometry, an unnecessary intersection of a face could occur. In this case, a blade moves away from the intersected face without changing a cutting point on the desired face. An example of the selected points and cutting angles is presented in Figure 18.

For clear understanding, we present a general simplified operation of the algorithm in Figure 19.

H. EFFECT OF THE RESOLUTION ON THE METHOD PERFORMANCE

We worked with the original image with a resolution of 3118 × 1778 pixels. This resolution turned out to be enough for correct operation; all stages were completed in 288.2 seconds. We decided to investigate the result and runtime depending on the reduced resolution. We reduced the resolution of the original image to 800 × 456 pixels and repeated the operation of our method. All stages were completed in 8.6 seconds; it is significantly faster. All faces and nodal points were found correctly on the test image, however, an imprecision increased.

The resolution of the original image is not of great importance. However, it is necessary to understand that low resolution can lead to errors in operation and reduce the precision of determining the coordinates of the nodal points, although it accelerates the runtime significantly. It is better to use images of the highest resolution in problem sites with a violation of geometry.

VI. RESULTS OF THE TEST TASKS SOLVING

The aluminum honeycomb block with a cell face length of 5 mm was cut for the practical test validation of the

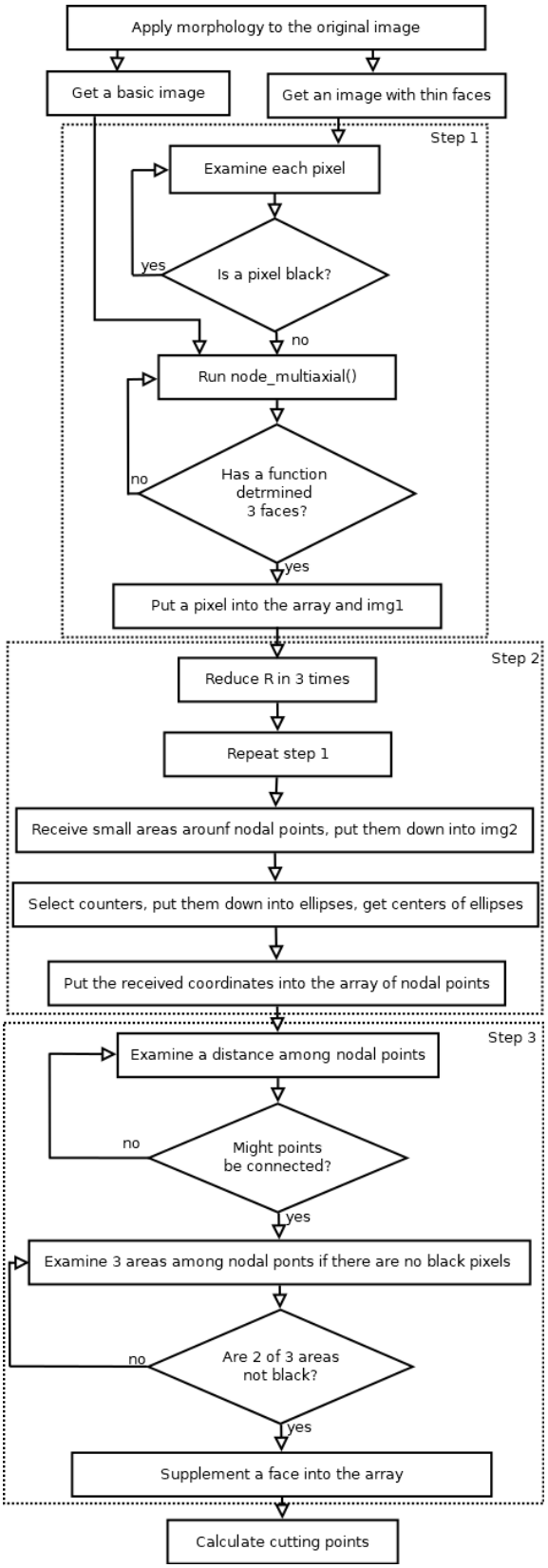

FIGURE 19. Diagram of the algorithm.

proposed method. The developed face cutter was attached to a CNC longitudinal milling tool. Also, a machine vision

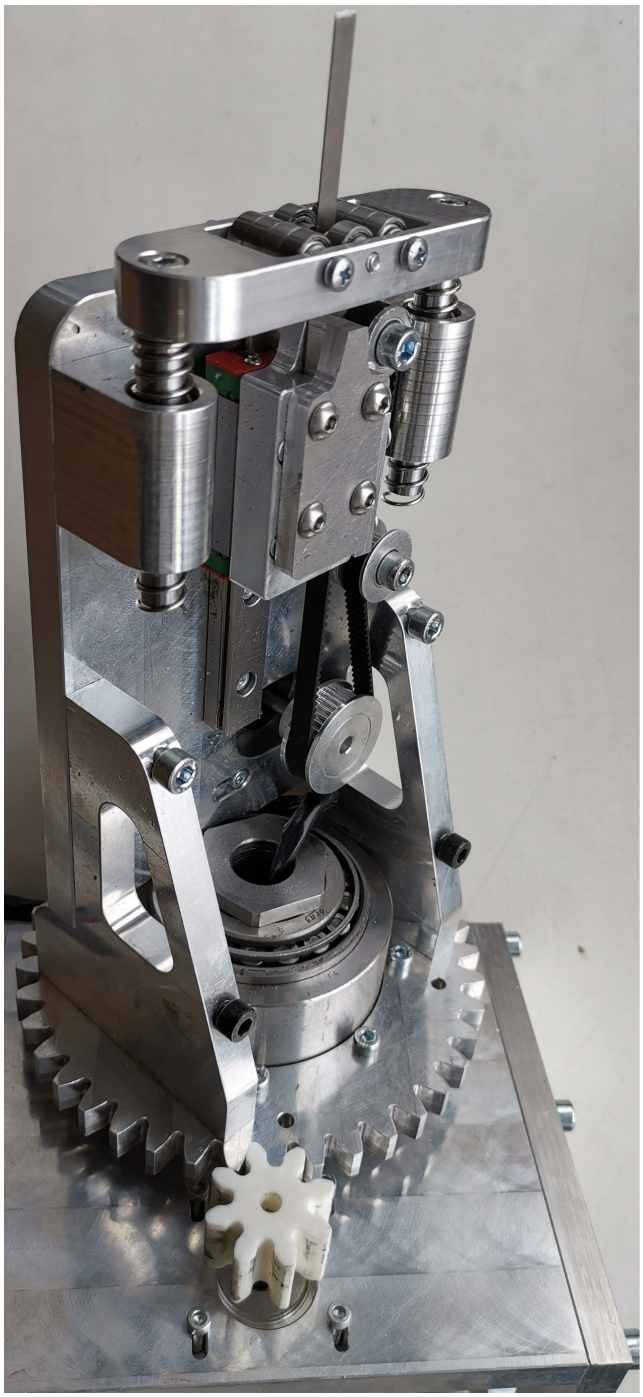

FIGURE 20. Cutter for faces cutting of the honeycomb block.

camera was fixed with the known shift relative to the central axis of the cutter. The cutter is shown in Figure 20.

The cutter has a rotating mechanism to set a given cutting angle. A pressure platform is implemented to fix the honeycomb block in the process of cutting and removing a blade. The platform is equipped with rotating rollers; the cutter can slide over the surface of the honeycomb block.

As a result of the experiment, the developed software determined coordinates and angles of the cut correctly and transferred them to the cutter. The cutter with the installed

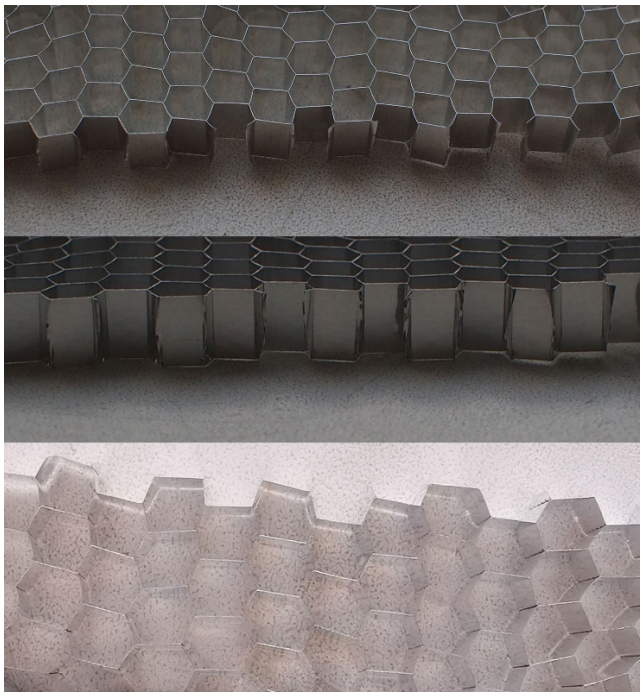

FIGURE 21. Result of the honeycomb block cutting.

tool carried out cutting of the honeycomb block in a given shape. The result is presented in Figure 21.

We conducted a study of the cut faces on a Neophot 32 microscope with the ability to measure distances on the resulting image. An example of one of the faces is shown in Figure 22. Measurements of the cut faces confirm the sufficiently high accuracy of the resulting cut, and, consequently, the correctness of machine vision systems and the operation of our method.

According to the presented image (Figures 21–22), coordinates are calculated correctly; the cut is performed correctly. There are closed cells and faces cut in 2 mm from the nodal points inside a cutting shape. This cutting method provides optimal strength characteristics for the cutting shape. Thus, it is possible to carry out precision cutting of the honeycomb block based on the obtained optimal cutting points with the minimum buckling.

The results were obtained while practical testing showed the high accuracy and reliability of the proposed method. The geometry of the honeycomb block was correctly recognized and cutting points and angles of the cutter were correctly determined in all test plots. We consider that this algorithm can be useful for a great variety of tasks when it is necessary to recognize faces and nodal points of cellular structures on an imperfect image. It does not have to be aluminum honeycomb block only or six-face structures. They can be cellular structures of any size and any material, with a lot of cell shapes (triangles, squares, polygons with different

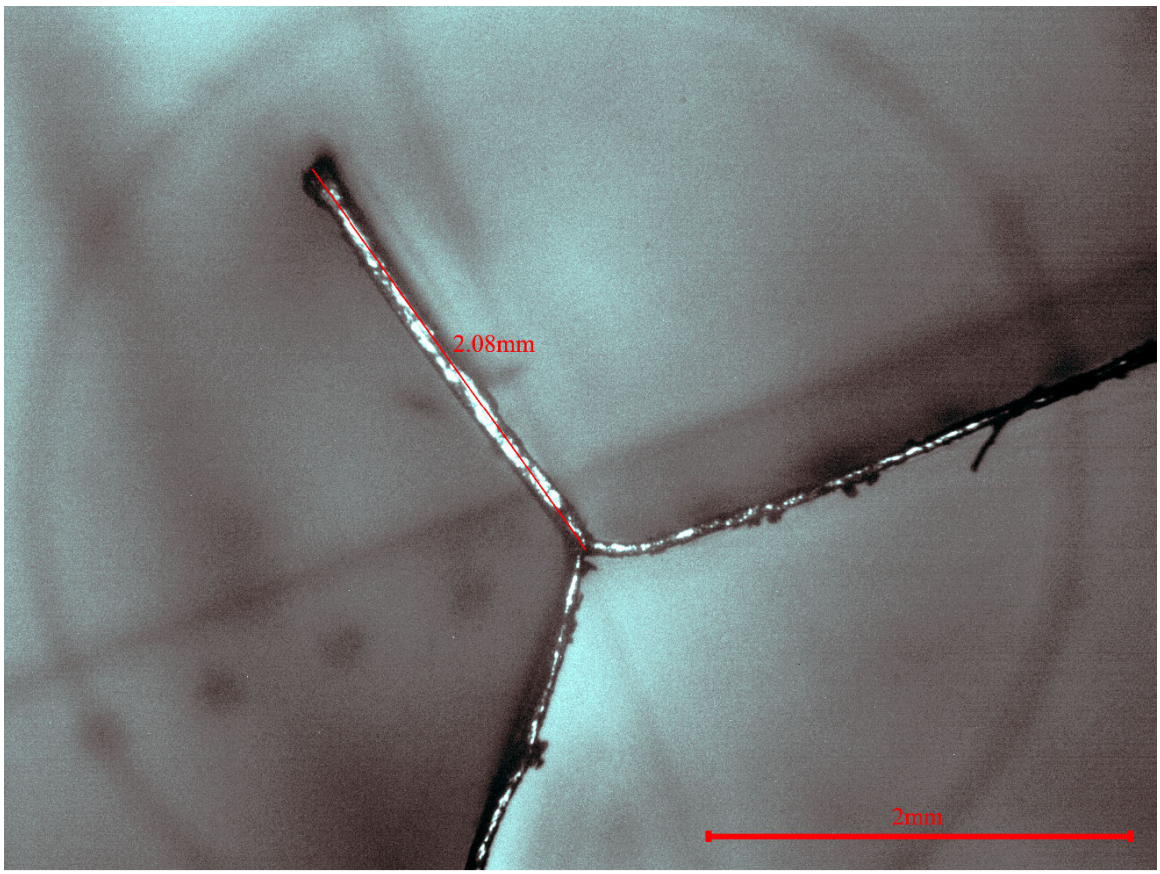

FIGURE 22. Microscope image of the cut face.

angles of connection at the nodal points). It is necessary only to change several variables for a specific task such as the number of faces connected at the nodal point, their average length and thickness in pixels. Depending on these features, the method will already select the remaining parameters such as a radius of the circle for the search, a step on the circle and other parameters. If it is necessary, it will be possible to modify the method to define more complex geometric structures, for example, with several types of nodal points, with a different number of faces converge. It is also possible to realize automatic determination of the recognized structure, the number and size of edges, and launch of the main method with already automatically optimally selected parameters.

VII. CONCLUSION

The calculations of stability and stretching force in the adjacent faces of the honeycomb block made it possible to determine the optimal plane of the face cut. The method for recognizing the faces and nodal points of honeycomb cores has been developed. It works correctly with an irregular honeycomb structure and geometry violations. The proposed method doesn't require high resolution of the processed image. The method finds nodal points and faces even in segments with significant defects, such as partially interrupted faces, local image exposures, irregular thickness and curved faces. The proposed method is applicable not only for the honeycomb block. It can be applied for some cellular cores by changing the corresponding variables. The number of faces converging at nodal points, an average length of a face, and deviations of geometric parameters influence the variables.

The proposed algorithm solves the problem of recognizing nodal points and faces of honeycomb blocks better than the existing algorithms included in the OpenCV library, and is more resistant to various image defects, curvature of faces and reduction in resolution. Also it can calculate optimal cutting points and angle; it is of significant practical importance for industries that use honeycomb cores. The developed method made it possible to solve the problem and obtain an automated system for cutting honeycomb blocks.

Therefore, a honeycomb core of the required shape with optimal strength and weight characteristics was obtained. Since a cut is carried out at optimal points, it is ensured that there are no slivers or supported faces. The practical verification has confirmed the correctness of the proposed method.

The application of the method proposed in the article will make it possible to obtain composite products of the improved quality with cellular cores. These products are currently in demand in the aerospace industry. Also, the application of the method significantly reduces human participation in the cutting process of honeycomb blocks due to the process of automation. It makes the result more predictable, repeatable and time consuming.

REFERENCES

[1] V. Crupi, G. Epasto, and E. Guglielmino, "Comparison of aluminium sandwiches for lightweight ship structures: Honeycomb vs. Foam," *Mar. Struct.*, vol. 30, pp. 74–96, Jan. 2013, doi: 10.1016/j.marstruc.2012.11.002.

[2] A. Boudjemai, M. H. Bouanane, A. Mankour, H. Salem, R. Hocine, and R. Amri, "Thermo-mechanical design of honeycomb panel with fully-potted inserts used for spacecraft design," in *Proc. 6th Int. Conf. Recent Adv. Space Technol. (RAST)*, Istanbul, Turkey, 2013, pp. 39–46, doi: 10.1109/RAST.2013.6581238.

[3] G. Bianchi, G. S. Aglietti, and G. Richardson, "Development of efficient and cost-effective spacecraft structures based on honeycomb panel assemblies," in *Proc. IEEE Aerosp. Conf.*, Big Sky, MT, USA, Mar. 2010, pp. 1–10, doi: 10.1109/AERO.2010.5446748.

[4] J. Wenjian, Z. Lanlan, W. Feng, S. Jinwen, and L. Yun, "Structural design and realization of a mechanical reconfigurable antenna," in *Proc. Int. Conf. Electron. Technol. (ICET)*, Chengdu, China, May 2018, pp. 349–353, doi: 10.1109/ELTECH.2018.8401401.

[5] K. A. Iyer, D. S. Mehoke, and R. C. Batra, "Interplanetary dust particle shielding capability of blanketed spacecraft honeycomb structure," in *Proc. IEEE Aerosp. Conf.*, Big Sky, MT, USA, Mar. 2017, pp. 1–10, doi: 10.1109/AERO.2017.7943909.

[6] L. Yan, H. Xu, and Y. Deng, "3D digital mockup for honeycomb sandwich panels of satellites," in *Proc. IEEE 4th Inf. Technol. Mechatronics Eng. Conf. (ITOEC)*, Chongqing, China, Dec. 2018, pp. 1956–1959, doi: 10.1109/ITOEC.2018.8740750.

[7] H. El Mir, M. Alkhader, P. D. Pour, and M. Mustafa, "Improving the buckling strength of honeycomb cores using periodic imperfections," in *Proc. Adv. Sci. Eng. Technol. Int. Conf. (ASET)*, Dubai, United Arab Emirates, Feb. 2020, pp. 1–6, doi: 10.1109/ASET48392.2020.9118353.

[8] E. Toth-Laufer and R. Horvath, "Mixed-order sugeno model to predict the resultant force in the milling process for honeycomb sandwich," in *Proc. IEEE 19th Int. Symp. Comput. Intell. Informat.*, Szeged, Hungary, Nov. 2019, pp. 131–136, doi: 10.1109/CINTI-MACRo49179.2019.9105124.

[9] D. Yip-Hoi, D. Gill, J. Gahan, G. Travis, and L. Mackaay, "Material stiffness and cutting parameters for honeycomb aluminum sandwich panel: A comparison with bulk material," *Procedia Manuf.*, vol. 34, pp. 385–392, Dec. 2019, doi: 10.1016/j.promfg.2019.06.182.

[10] X. Li, Y. Lin, F. Lu, and Y. Zhang, "Quasi-static cutting response of combined hexagonal aluminium honeycombs at various stacking angles," *Compos. Struct.*, vol. 238, Apr. 2020, Art. no. 111942, doi: 10.1016/j.compstruct.2020.111942.

[11] K. Sanjay, V. Sabareeshsun, S. Govindan, K. Reena, M. Saravannan, and A. J, "Automated honeycomb composite structure repair system," in *Proc. 6th Int. Conf. Adv. Comput. Commun. Syst. (ICACCS)*, Coimbatore, India, Mar. 2020, pp. 276–279, doi: 10.1109/ICACCS48705.2020.9074193.

[12] M. Batool, A. M. Khan, H. S. U. Butt, and N. Saeed, "Geometric sensitivity of static equivalent modeling techniques for honeycomb cores," in *Proc. 6th Int. Conf. Aerosp. Sci. Eng. (ICASE)*, Islamabad, Pakistan, Nov. 2019, pp. 1–6, doi: 10.1109/ICASE48783.2019.9059200.

[13] M. Ke, Z. Jianfu, F. Pingfa, W. Zhijun, Y. Dingwen, and S. Ahmad, "Design and implementation of a mini ultrasonic cutting system for nomex honeycomb composites," in *Proc. 16th Int. Bhurban Conf. Appl. Sci. Technol. (IBCAST)*, Islamabad, Pakistan, Jan. 2019, pp. 148–152, doi: 10.1109/IBCAST.2019.8667261.

[14] K. Qiu, W. Ming, L. Shen, Q. An, and M. Chen, "Study on the cutting force in machining of aluminum honeycomb core material," *Compos. Struct.*, vol. 164, pp. 58–67, Mar. 2017, doi: 10.1016/j.compstruct.2016.12.060.

[15] X. P. Hu, B. H. Yu, X. Y. Li, and N. C. Chen, "Research on cutting force model of triangular blade for ultrasonic assisted cutting honeycomb composites," *Procedia CIRP*, vol. 66, pp. 159–163, Dec. 2017, doi: 10.1016/j.procir.2017.03.283.

[16] J. Sun, Z. Dong, X. Wang, Y. Wang, Y. Qin, and R. Kang, "Simulation and experimental study of ultrasonic cutting for aluminum honeycomb by disc cutter," *Ultrasonics*, vol. 103, Apr. 2020, Art. no. 106102, doi: 10.1016/j.ultras.2020.106102.

[17] G. Tiwari, T. Thomas, and R. P. Khandelwal, "Influence of reinforcement in the honeycomb structures under axial compressive load," *Thin-Walled Struct.*, vol. 126, pp. 238–245, May 2018, doi: 10.1016/j.tws.2017.06.010.

[18] E. Perumal and P. Arulandhu, "Multilevel morphological fuzzy edge detection for color images (MMFED)," in *Proc. Int. Conf. Electr., Electron., Commun., Comput., Optim. Techn. (ICEECCOT)*, Mysuru, Karnataka, Dec. 2017, pp. 269–273, doi: 10.1109/ICEECCOT.2017.8284680.

[19] J. Wu, Z. Yin, and Y. Xiong, "The fast multilevel fuzzy edge detection of blurry images," *IEEE Signal Process. Lett.*, vol. 14, no. 5, pp. 344–347, May 2007, doi: 10.1109/LSP.2006.888087.

[20] J. Lu, H. Pan, and Y. Xia, "The weld image edge-detection algorithm combined with Canny operator and mathematical morphology," *Proc. 32nd Chin. Control Conf.*, Xi'an, China, 2013, pp. 4467–4470.
[21] G. Deng and Y. Wu, "Double lane line edge detection method based on constraint conditions Hough transform," in *Proc. 17th Int. Symp. Distrib. Comput. Appl. for Bus. Eng. Sci. (DCABES)*, Wuxi, China, Oct. 2018, pp. 107–110, doi: 10.1109/DCABES.2018.00037.
[22] M. V Kubrikov, I. A Paulin, M. V Saramud, and A. S Kubrikova, "Application of sequential processing of computer vision methods for solving the problem of detecting the edges of a honeycomb block," 2020, *arXiv:2010.13837*. [Online]. Available: http://arxiv.org/abs/2010.13837
[23] *Hough Line Transform*. Accessed: Dec. 30, 2020. [Online]. Available: https://docs.opencv.org/3.4/d9/db0/tutorial_hough_lines.html
[24] *Harris Corner Detector*. Accessed: Dec. 30, 2020. [Online]. Available: https://docs.opencv.org/3.4/d4/d7d/tutorial_harris_detector.html
[25] *Harris Corner Detection*. Accessed: Dec. 30, 2020. [Online]. Available: https://docs.opencv.org/3.4/dc/d0d/tutorial_py_features_harris.html
[26] *Shi-Tomasi Corner Detector*. Accessed: Dec. 30, 2020. [Online]. Available: https://docs.opencv.org/3.4/d8/dd8/tutorial_good_features_to_track.html
[27] *FAST Algorithm for Corner Detection*. Accessed: Dec. 30, 2020. [Online]. Available: https://docs.opencv.org/master/df/d0c/tutorial_py_fast.html
[28] *Femap*. Accessed: Dec. 30, 2020. [Online]. Available: https://www.plm.automation.siemens.com/global/ru/products/simcenter/femap.html
[29] V. Balambica and V. Deepak, "Static analysis of slotted springs," in *Proc. Int. Conf. Autom. Control Dyn. Optim. Techn. (ICACDOT)*, Pune, Italy, Sep. 2016, pp. 455–459, doi: 10.1109/ICACDOT.2016.7877627.

MAKSIM V. KUBRIKOV received the degree in technical sciences (design, construction and production of aircraft) from the Siberian State Aerospace University, in 2011. He is currently a Leading Researcher with the Research Laboratory of Robotic Systems, Reshetnev Siberian State University of Science and Technology. His research interests include automation, robotics, cyber-physical systems, and additive technologies.

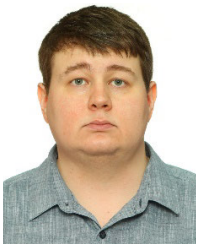

MIKHAIL V. SARAMUD received the degree in technical sciences (system analysis, control theory, and information processing) from the Reshetnev Siberian State University of Science and Technology, in 2018. He is currently a Senior Researcher with the Research Laboratory of Robotic Systems, Reshetnev Siberian State University of Science and Technology, and also an Associate Professor with the Department of Informatics, Institute of Space and Information Technologies, Siberian Federal University. His research interests include software reliability, robotics, system analysis, optimization, and simulation modeling.

MARGARITA V. KARASEVA received the degree in technical sciences (system analysis, control theory, and information processing), in 2002. She is currently an Associate Professor with the Department of Systems Analysis and Operations Research, Reshetnev Siberian State University of Science and Technology, and the Department of Digital Technologies of Management, School of Business Management and Economics, Siberian Federal University. Her main research interests include connected with information technologies and multilinguistics.